Geochimica et Cosmochimica Acta, Vol. 69, No. 21, pp. 5005–5019, 2005

0016-7037/05 $30.00 + .00

doi:10.1016/j.gca.2005.04.026

Modeling the impact of microbial activity on redox dynamics in porous media

Martin Thullner,*,† Philippe Van Cappellen, and Pierre Regnier
Department of Earth Sciences—Geochemistry, Utrecht University, PO Box 80021, 3508TA Utrecht, The Netherlands

(*Received December* 6, 2004; *accepted in revised form April* 25, 2005)

Abstract—The present study investigates the interaction between microbial growth and activity and the redox dynamics in natural porous media. The impact the transport regime has on this interaction is also addressed. Expressions for microbial growth are incorporated into a geochemical reaction network linking redox reaction rates to the activity of the microorganisms. A flexible simulation environment, the Biogeochemical Reaction Network Simulator (BRNS) is used for this purpose. Two reactive transport applications relevant to fields of contaminant hydrology and early diagenesis are simulated with the BRNS. Model results are evaluated based on a comparison with comprehensive datasets on the biodegradation of lactate in a sand column experiment and on the distribution of redox-sensitive chemical species in marine sediments of the Skagerrak, Denmark. It is shown that, despite quite different transport regimes, the geomicrobiological model performs equally well in the reproduction of measured chemical species distribution for both applications. This result emphasizes the broad applicability of the proposed approach. Our simulations support that the competitive behavior between various microbial groups is a process controlling the development of redox stratified environments. Furthermore, it is also shown that the transport regime is a key controlling factor for the degree of spatial correlation between microbial biomass distributions and redox reaction rates. Although all our simulations yield a pronounced stratification of the redox processes in the system, the biomass distribution is related to the associated reaction rates only in case of the advection controlled column experiment. In the early diagenetic application, mixing due to bioturbation is the dominant transport process for particulate matter, hence leading to fairly homogeneous distribution of bacterial biomasses which are unrelated to the spatial distribution of redox reaction rates. This homogeneous biomass distribution combined with the 1G carbon degradation model approach might explain why the steady state concentration profiles in such systems can be reproduced by diagenetic models without explicit representation of microbial growth.

1. INTRODUCTION

A large variety of reactive processes in porous media are directly or indirectly driven by the microbially-mediated degradation of organic carbon. Even though the source, composition and reactivity of organic matter are highly variable in natural environments, the overall process of degradation often results in a characteristic zonation of redox conditions. This zonation is explained by utilization of terminal electron acceptors (TEAs) involved in organic carbon degradation reactions in a temporal or, where transport is considered, spatial sequence of decreasing energy yields (Chapelle, 1992; Appelo and Postma, 1993). The dynamics, however, of redox-stratified environments are complicated by additional, secondary redox reactions, which involve the TEAs and the reduced end-products of the primary redox processes (e.g., Van Cappellen and Wang, 1996; Hunter et al., 1998).

The interaction of redox transformations with transport processes is another important feature controlling the chemical zonation of natural systems. In aquifers, for instance, transport of dissolved chemical species percolating through an immobile solid matrix is dominated by advective flow velocities up to 100 m y^{-1} and more (e.g., Harter, 2003). In aquatic sediments, transport of solids occurs mainly via burial and bioturbation. Advection velocities associated with burial are typically on the order of 10^{-2} m y^{-1} or less (Van Cappellen and Gaillard, 1996; Middelburg et al., 1997). For this reason, molecular diffusion and particulate mixing by bioturbation are often the dominant mechanisms of transport in such environments.

The nature and relative magnitude of transport processes not only determines the spatial and temporal distributions of dissolved and solid redox-sensitive chemical species, but also those of reaction rates and the microbial community structure. Subsurface microorganisms are typically particle bound (typically grow at the solid-solution interface), leading to the formation of a biophase (biofilm or aggregates). Thus, the transport, or absence thereof, of solids may contribute to the spatial structuring of redox processes in natural environments.

In recent years, advances in molecular biology have provided novel insights on the microbial processes driving redox dynamics in porous media environments. New tools have been used to quantify and characterize microorganisms in aquifers and sediments (e.g., Hess et al., 1996; Zarda et al., 1998; Wieringa et al., 2000) and experimental studies elucidating the spatial distribution of bacteria are now being conducted on a routine basis (e.g., Roose-Amsaleg et al., 2001). Among others, such studies have been used to predict in situ redox reaction rates (e.g., Sass et al., 1997; Ravenschlag et al., 2000), even though the relationship between microbial abundance and redox reaction rates remains unclear. This is certainly a research question that deserves more attention.

Reactive-Transport Models (RTMs) are particularly suitable tools for capturing the complex interplay between the microbial

* Author to whom correspondence should be addressed (martin.thullner@ufz.de).
† *Present address*: Department of Environmental Microbiology, UFZ—Center of Environmental Research Leipzig-Halle, Permoserstr. 15, 04318 Leipzig, Germany.

community structure and chemistry of redox-stratified environments. To date, however, the integration of microbial ecology into RTMs remains sketchy. A succinct review of the state-of-the art in the field of reactive transport modeling is thus particularly useful, as it clearly points the way to future developments.

In contaminant hydrology, RTMs are commonly used to simulate the transient behavior of redox-sensitive chemical species at time scales ranging from a few hours to several decades. Although the coupling of redox rates to microbial dynamics is often considered to be essential in this field (Smets and Pritchard, 2003), simulations involving a large set of hydrochemical processes in aquifers often do not incorporate rate formulations explicitly controlled by microbial activity (e.g., Hunter et al., 1998; van Breukelen et al., 2004). In contrast, applications focusing exclusively on the fate of organic contaminants generally couple the rates of the primary redox reactions to the growth and activity of specific microbial groups (e.g., reviews by Murphy and Ginn, 2000; Barry et al., 2002; Brun and Engesgaard, 2002; and literature cited therein). In such studies, however, the hydrochemical reaction network, including secondary redox reactions, is often seriously limited. Noteworthy exceptions include the recent modeling studies of Schäfer et al. (1998a), Mayer et al. (2002), and Prommer et al. (2003), which combine microbially mediated reactive processes with a comprehensive set of abiotic (hydro)geochemical reactions.

In the field of early diagenetic modeling, the focus is mainly on the simulation of the steady state vertical distributions of chemical concentrations and reaction rates. RTMs often include a large variety of geochemical processes such as redox reactions, homogeneous acid-base equilibria, and the precipitation-dissolution of mineral phases (e.g., Boudreau, 1996; Soetaert et al., 1996; Van Cappellen and Wang, 1996; Berg et al., 2003). Yet, these models rarely include explicit expressions for microbial growth and, as a result, the dependency of redox reaction rates on changes in microbial community structure is not represented specifically. Some exceptions exist (e.g., Talin et al., 2003; Baurmann et al., 2004), but these studies are mainly on the conceptual level, and only implement highly simplified reaction networks. In addition, many of the widely applied RTMs (e.g., STEADYSED (Van Cappellen and Wang, 1996), CANDI (Boudreau, 1996)) have been used successfully to reproduce measured concentration profiles, but are based on rate expressions for primary redox processes where ad hoc formulations regulate the succession of the degradation pathways of organic matter. Accumulating evidence shows that these pathways may overlap (e.g., Jakobsen and Postma, 1999). For instance, incubation experiments have demonstrated that reactive Fe(III)-oxyhydroxides, a more favorable TEA, does not inhibit sulfate-reduction when electron donors are present in high abundance (Koretsky et al., 2003). These results indicate that, alternative model approaches, based on competition between microbial groups, may be more appropriate to explain and predict patterns of redox activity in subsurface environments.

In this paper, microbial growth kinetics are integrated in a geochemical reaction network model for redox dynamics using a flexible simulation environment (Biogeochemical Reaction Network Simulator or BRNS; Regnier et al., 2002). This modeling tool is appropriate to investigate biogeochemical transformations in complex reaction environments, characterized by a large range of spatio-temporal scales and transport regimes. Reaction networks of arbitrary size and complexity can be defined and coupled to 1D transport processes (Regnier et al., 2003; Aguilera et al., 2005). The applicability of the model is tested using two classical literature examples in the area of contaminant hydrology and early diagenesis, which have been modeled previously by Schäfer et al. (1998b) and Wang and Van Cappellen (1996), respectively. Expressions used to simulate microbial dynamics and their effects on redox reaction rates are validated using the first example, which is based on the detailed results of a column experiment by von Gunten and Zobrist (1993). A mechanistic representation of the primary redox reactions is proposed, where microbial competition for the organic energy substrates leads to the formation of a redox sequence. The resulting microbially-driven reaction network is then applied to the early diagenesis example (Canfield et al., 1993), to determine whether the proposed rate expressions are suitable to simulate organic matter degradation in nearshore marine sediments.

Overall, the aim of this study is to verify if our model is applicable to reactive transport problems characterized by different transport regimes and to evaluate the sensitivity of the simulation results towards using different kinetic models for microbially driven reactions. In addition, we investigate the extent to which the spatial distribution of microbial groups relates to the corresponding redox reaction rates, and how this relationship is influenced by transport processes.

2. MODEL DESCRIPTION

The mathematical formulation of the Biogeochemical Reaction Network Simulator (BRNS), which is used here to compute transient and steady-state redox dynamics in porous media is described in detail in Regnier et al. (2002, 2003) and Aguilera et al. (2005). Briefly, the simulation environment consists of a generalized finite difference algorithm for one-dimensional advection-diffusion coupled to a multi-component reaction solver capable of handling mixed kinetic-equilibrium systems. The transport and reaction components are solved in sequence within a single time step of numerical integration, following the Sequential Non-Iterative Algorithm (SNIA, Steefel and MacQuarrie, 1996). The simultaneous occurrence of kinetic and equilibrium reactions leads to a non-linear set of differential algebraic equations (DAE, Brenan et al., 1989; Hindmarsh and Petzold 1995a, 1995b), which is solved iteratively by the Newton-Raphson method (Press et al., 1992), after a preprocessing step as described in Regnier et al. (2002). The method employs a first degree Taylor series expansion to linearize the equations at every single iteration step.

In the BRNS, the function residuals, which represent the reaction network, and the Jacobian matrix, which contains the partial derivatives of the function residuals with respect to the unknown concentrations, are automatically assembled and translated into source code specific to each RTM application, hence offering full flexibility. This procedure is implemented in MAPLE symbolic programming language (Chilakapati, 1995; Regnier et al., 1997). Detailed examples of the automated procedure are given in Regnier et al. (2002). The Jacobian

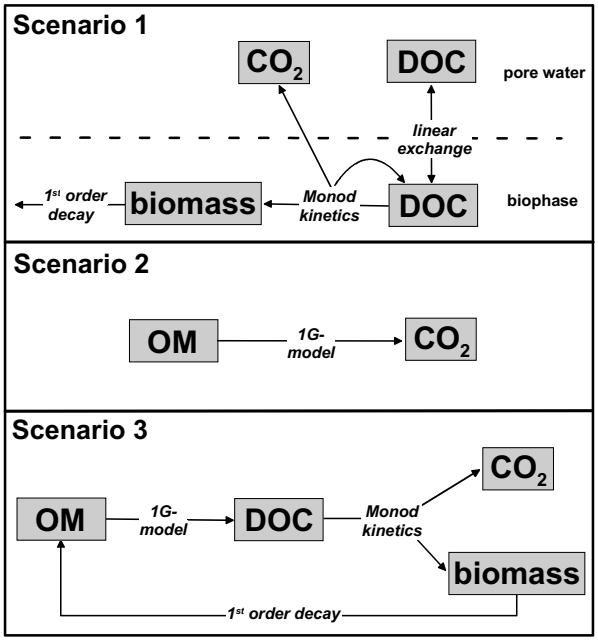

Fig. 1. Organic carbon flows simulated in the different scenarios. The TEAs driving carbon oxidation are determined by the kinetic parameters of Eqn. 1 (Scenarios 1 and 3) or by the limiting concentrations of Eqn. 2 (Scenario 2). OM: organic matter; DOC: dissolved organic carbon.

matrix and the function residuals, plus all user-dependent information (e.g., initial and boundary conditions, transport coefficients, etc.) are translated into fully structured FORTRAN code using the MACROFORT package (Gomez, 1990) and our own library of MAPLE procedures (ACGLIB). The resulting routines are then linked with a numerical engine, which contains standard routines for solving the transport equations and the coupled nonlinear process equations generated by the MAPLE preprocessor (linear algebra solver). The model outputs provide concentrations (including biomasses) and reaction rates at any grid point of the discretized spatial domain, as well as material fluxes through any cell interface.

3. SCENARIOS

Two comprehensive data sets, from the fields of contaminant hydrology (von Gunten and Zobrist, 1993) and from early diagenesis (Canfield et al., 1993) were used to assess model performance and to allow a comparison between systems characterized by different transport regimes. The first data set was compared with simulations based on a reaction network explicitly linking redox dynamics to microbial growth (Scenario 1). Two different scenarios of increasing complexity were then considered in the early diagenetic application, one without (Scenario 2) and one with (Scenario 3) explicit representation of microbial growth in the degradation pathways of organic carbon (primary redox processes). A schematic representation of the flows between the various carbon pools implemented in the three scenarios is given in Figure 1 using stoichiometries and reaction rates as described in the Appendix. In addition to the primary redox processes, the reaction network considered for the different scenarios included also secondary redox processes, mineral precipitation/dissolution reactions and acid-base equilibria (Table 1). Our simulations provided concentration profiles for all major redox-sensitive species, rate distributions and a complete carbon mass balance.

3.1. Scenario 1: Organic Carbon Degradation in a Sand Column Experiment

To investigate the degradation potential of organic contaminants in groundwater environments, column experiments are often used. These experimental model systems allow one to study microbial process kinetics under dynamic flow conditions. Thus, for the first scenario, we selected a column experiment designed to simulate the microbial response to the supply of labile organic substrates. In this experiment, artificial groundwater containing lactate as electron donor as well as oxygen, nitrate and sulfate as TEAs was constantly pumped through a 29 cm long water saturated sand column containing solid phase manganese and iron oxyhydroxides as additional TEAs on the sand matrix. In the experimental, advection-dominated, transport regime Peclet numbers typically reached a value of 10 at the cm-scale. Longitudinal concentration profiles of dissolved chemical species were monitored throughout the experiment, while matrix bound concentrations were measured at the end of the experiment (day 110). The results indicated that the highest microbial activity, and thus, highest organic carbon degradation rates occurred near the column inlet. The concentration profiles implied that lactate was mineralized directly into dissolved inorganic carbon (DIC), as well as fermented to acetate and propionate, the latter intermediate being further oxidized into DIC. The experiment is described in detail as "column 2" in von Gunten and Zobrist (1993).

The dataset was already used in the modeling work of Schäfer et al. (1998b), who considered a reaction network of more than 20 reactions, 30 reactive species, and five microbial groups (Table 1). In their study, the growth of microorganisms involved in the primary redox reactions was expressed using a first-order dependency with respect to bacterial biomass and Monod terms for the electron donor and acceptor (Monod, 1949):

$$\frac{\partial B_i}{\partial t} = \left(\sum_j \mu_{i,j} \cdot \frac{c_{DOC_{i,j}}}{K_{DOC_{i,j}} + c_{DOC_{i,j}}} \frac{c_{TEA_{i,j}}}{K_{TEA_{i,j}} + c_{TEA_{i,j}}} \cdot \frac{K_{inh_{i,j}}}{K_{inh_{i,j}} + c_{O_2}} \right) \cdot B_i \quad (1)$$

In Eqn. 1, B_i represents the bacterial biomass concentration and $\mu_{i,j}$ the maximum growth rate of microbial group i using TEA j, c_{DOC} and c_{TEA} are the respective concentrations of organic carbon substrate and TEA used by each microbial group, and K_{DOC} and K_{TEA} are the corresponding half-saturation constants. Schäfer et al. (1998b) hypothesized that a single group of facultative anaerobes could use both oxygen and nitrate as their TEA, that is, for this microbial group $j = 1$ to 2. For all other microbial groups, j was set to 1, meaning that these bacteria could only grow on a single electron acceptor, namely iron, manganese, or sulfate. Oxygen was assumed to inhibit all anaerobic degradation processes; K_{inh} is the inhibition constant of oxygen and c_{O_2} is the oxygen concentration. No further

Table 1. Reaction networks implemented in the different scenarios. Processes given in *italics* are defined by their thermodynamic equilibrium constraints. Apparent equilibrium constants were used for Scenarios 2 and 3 to include nonspecific and specific (aqueous complexes) interactions. All other reactions are defined by kinetic rates laws.

Reaction type	Groundwater column (Scenario 1)	Sediment core (Scenarios 2 and 3)
Primary redox reactions	• oxidation of lactate by oxygen and nitrate • fermentation of lactate (producing propionate and acetate) • oxidation of propionate by Mn(IV), Fe(III) and sulfate	• oxidation of DOC by oxygen, nitrate, Mn(IV), Fe(III) and sulfate
Secondary redox reactions	• oxidation of sulfide by Fe(III)	• oxidation of ammonium, sulfide, Mn(II) and Fe(II) by oxygen • oxidation of Fe(II) by Mn(IV) • oxidation of sulfide by Mn(IV) and Fe(III) • oxidation of FeS by oxygen
Non-redox reactions	• Precipitation/dissolution of Fe(II)-minerals • *Precipitation/dissolution of calcite* • *Acid-base reactions for carbonates, sulfides, lactate, propionate and acetate*	• Precipitation/dissolution of Mn(II)- and Fe(II)-minerals • *Acid-base reactions for carbonates and sulfides* • *Adsorption of ammonium, Mn(II) and Fe(II)*
Reactive species	• 5 microbial groups • lactic acid, propionic acid, acetic acid, lactate, propionate and acetate • oxygen, nitrate, Mn(IV), Fe(III) and sulfate • dissolved Mn(II) and Fe(II) • Fe(II)-minerals • H^+ • carbonates and sulfides	• 4 microbial groups (Scenario 3, only) • organic matter • dissolved organic carbon (Scenario 3, only) • oxygen, nitrate, Mn(IV), Fe(III), sulfate • dissolved ammonium, Mn(II) and Fe(II) • adsorbed ammonium, Mn(II) and Fe(II) • Mn(II)- and Fe(II)-minerals • H^+ • carbonates and sulfides

inhibition was assumed in the model formulation. The fifth microbial group consisted of fermenters, for which the Monod term with respect to the TEA in Eqn. 1 was neglected.

The consumption of organic carbon substrates, terminal electron acceptors, and the release of reaction products were related to the growth of each microbial group using specific yield factors, Y_i, combined with the stoichiometry of the individual primary redox reactions. The decay of microorganisms was simulated assuming first order kinetics with respect to the bacterial biomass. A recycling of the dead biomass was not considered.

The reaction network proposed by Schäfer et al. (1998b) was implemented in the BRNS. Schäfer et al. (1998b) further assumed that all microbial processes occur in a biofilm or biophase occupying a small fraction of the pore space. Detachment of biomass was considered to be negligible, and the exchange of chemical species between the biophase and the pore water or sand matrix was described by an exchange term of the form $\frac{\partial m}{\partial t} = \alpha(c_{bio} - c_{pore/matrix})$, with m as the exchanged mass per total sediment volume, α as a rate parameter, and c_{bio} and $c_{pore/matrix}$ as species concentration in the biophase and in the pore water or on the matrix, respectively. The pore water, sand matrix, and biophase were assumed to be chemically homogeneous within each grid cell.

A detailed description of the reaction network and associated parameters is given in Schäfer et al. (1998b). The same set of processes and parameter values were used in the present study. Schäfer et al. (1998b) performed their numerical simulations using a spatial discretization of 3.9 mm and a time step size of 10^{-2} days. Although these discretizations led to a Courant number of approximately 2, we decided, for the sake of comparison, to keep these values in our simulations. In addition, test runs with smaller time steps did not lead to significantly different results.

3.2. Scenario 2: Carbon Cycling in Coastal Sediments—Geochemical Model

For the second scenario, a data set collected in coastal sediments from the eastern Skagerrak off the coast of Denmark was used. In this environment, fresh organic matter reaching the sediment water interface is oxidized by dissolved (oxygen, nitrate, sulfate) and solid phase (manganese and iron oxides) TEAs. Diffusion and bioturbation are the most important transport processes for dissolved and solid species, respectively, with Peclet numbers smaller than 0.01 on a cm-scale. The concentrations of the TEAs are not only controlled by the organic matter degradation pathways but also by other biogeochemical reactions, such as the reoxidation of reduced inorganic species, and mineral precipitation and dissolution. As a result of the progressive breakdown of deposited organic mat-

Table 2. Parameter values used for the simulation of Scenarios 2 and 3 which differ from those used by Wang and Van Cappellen (1996). J_{OM}, J_{fe} and J_{mn} are the fluxes of organic matter, solid Fe(III) and solid Mn(IV) reaching the sediment-water interface; k_C is the decay rate constant of organic matter (1G model). The other parameters are rate constants using the nomenclature of Wang and Van Cappellen (1996): *k10:* aerobic oxidation of adsorbed Fe(II); *k22:* precipitation of $MnCO_3$; *k23:* precipitation of $FeCO_3$; *k24:* precipitation of FeS. α_0 is the rate constant for non-local exchange due to bioirrigation.

Parameter	Units	Wang and Van Cappellen (1996)	Scenario 2	Scenario 3 "reference case"	Scenario 3 "high activity case"
J_{OM}	μmol cm^{-2} y^{-1}	—	660	650	635
J_{fe}	μmol cm^{-2} y^{-1}	75	68	71	60
J_{mn}	μmol cm^{-2} y^{-1}	40	32	28	28
k_C	y^{-1}	—	0.95	0.95	0.95
k10	M^{-1} y^{-1}	$5 \cdot 10^{7}$	$1 \cdot 10^{7}$	$1 \cdot 10^{7}$	$1 \cdot 10^{7}$
k22	mol g^{-1} y^{-1}	$1 \cdot 10^{-4}$	$6 \cdot 10^{-5}$	$6 \cdot 10^{-5}$	$6 \cdot 10^{-5}$
k23	mol g^{-1} y^{-1}	$4.5 \cdot 10^{-4}$	$4.9 \cdot 10^{-4}$	$5.4 \cdot 10^{-4}$	$5.4 \cdot 10^{-4}$
k24	mol g^{-1} y^{-1}	$1.5 \cdot 10^{-5}$	$3.3 \cdot 10^{-5}$	$2.3 \cdot 10^{-5}$	$3.2 \cdot 10^{-5}$
α_0	y^{-1}	200[a]	190	190	190

[a]Taken from Van Cappellen and Wang (1996)

ter, the sediments exhibit the generally observed vertical redox zonation. A complete description of the data set is given as "core S4" in Canfield et al. (1993).

The data set from core S4 was used in the modeling studies of Van Cappellen and Wang (1996) and Wang and Van Cappellen (1996). A reaction network of more than 20 biogeochemical reactions (Table 1) was included in their work. The simulations successfully reproduced the main features of the measured vertical concentration profiles. In their study, all reaction rates, including those describing the primary redox reactions, were assumed to depend on the concentration of chemical reactants only, and no explicit link between microbial activity and reaction rates was in the kinetic expressions. In fact, the total carbon oxidation rate was used as a forcing function rather than as a model output. The contribution of each metabolic pathway, f_i, to the total carbon oxidation rate was defined according to:

$$f_i = \left(1 - \sum_{j<i} f_j\right) \cdot 1 \text{ if } c_{TEA,i} > c_{lim,i} \text{ and } f_i = \left(1 - \sum_{j<i} f_j\right) \cdot \frac{c_{TEA,i}}{c_{lim,i}} \text{ if } c_{TEA,i} < c_{lim,i} \quad (2)$$

where the order, i, of TEAs is O_2 ($i = 1$), NO_3 ($i = 2$), MnO_2 ($i = 3$), $Fe(OH)_3$ ($i = 4$), SO_4 ($i = 5$). In Eqn. 2, $c_{lim,i}$ is a threshold (or limiting) concentration which controls the transition from one metabolic pathway to the other. That is, a sufficiently high concentration of a given TEA, $c_{TEA,i}$, completely inhibits all other, less favorable metabolic pathways.

The reaction network and the rate laws of Van Cappellen and Wang (1996) and Wang and Van Cappellen (1996) were incorporated in the BRNS using identical parameter values except for those listed in Table 2. The main difference between the present and previous study lies in the description of the rate of organic carbon mineralization. Instead of a forcing function, the total carbon oxidation rate was simulated here to allow an easier comparison with results of Scenario 3. We used the simplest possible kinetic description, namely a first order rate law with respect to a single pool of organic matter, following the 1G-model approach of Berner (1980):

$$\frac{\partial c_{OM}}{\partial t} = k_c c_{OM} \quad (3)$$

where c_{OM} is the concentration of degradable organic matter (OM), and k_c is the first order rate constant. The contributions of the various metabolic pathways of organic matter degradation were determined using Eqn. 2. The simulations performed by Van Cappellen and Wang (1996) and Wang and Van Cappellen (1996), comprised only the uppermost 20 cm of sediment discretized using a uniform, 1 mm grid. Since the assumption of a zero gradient boundary condition at 20 cm used by these authors for dissolved and solid iron and manganese species was not verified by test runs performed with our model, a maximum depth of 100 cm with variable spatial discretization was used instead. We applied depth intervals ranging from 1 mm at the sediment water interface to 2.5 cm at the largest depth. Thus, a possible reason for deviations between the simulation results presented here and those of Wang and Van Cappellen (1996) is the greater depth of the lower boundary used in our study. The latter also explains why different parameters had to be applied for the description of iron and manganese cycling (Table 2).

In the present study, transient simulations were performed using a time step interval of 10^{-5} years until steady state was reached. In test runs, a further refinement of the time steps did not produce changes in the simulation results. Besides the differences described above, all other processes and parameters were simulated as described by Van Cappellen and Wang (1996) and Wang and Van Cappellen (1996).

3.3. Scenario 3: Organic Carbon Cycling in Coastal Sediments—Geomicrobial Model

In this simulation, the reaction network presented in Scenario 2 was expanded to link the rates of primary redox reactions to the activity of four different microbial groups (facultative aerobic or nitrate reducers, Mn(IV) reducers, Fe(III) reducers, and sulfate reducers). These groups are identical to those used in Scenario 1, except for the fermentative group, which was ignored here. The 1G-model of organic matter degradation was modified to include first-order hydrolysis of the macromolecular organic matter into an intermediate DOC pool, which serves as an energy and carbon substrate to the microorganisms (Fig. 1). The microorganisms were assumed to be associated to the solid phase and, therefore, were affected by the processes of

Table 3. Scenario 3: Parameter values used for the simulation of bacterial growth ("Reference case"). The decay rate constant is set to $\mu_{dec}=0.1$ y^{-1} and the half saturation constant for DOC is $K_{DOC}=1$ μM for all bacterial groups. Note that the limiting concentrations given in the last column are shown only for comparison and refer to reaction rate expressions excluding bacterial growth.

Bacterial group	Maximum growth rate; μ_i [y^{-1}]	Half saturation constant for TEAs; K_i [μM] for dissolved or [μmol g^{-1}] for solid state TEAs	Inhibition constant for oxygen; $K_{inh,i}$ [μM]	Yield factor; Y_i [mol $C_{biomass}$ per mol C_{DOC}]	Limiting concentration used by Wang and Van Cappellen (1996) [μM or μmol g^{-1}]
Facultative aerobes (with oxygen)	10	20	—	0.20	20
Facultative aerobes (with nitrate)	7.5	5	20	0.15	5
Manganese reducers	7.5	1.6*	200	0.15	16*
Iron reducers	2.5	1.0*	200	0.05	100*
Sulfate reducers	2.0	1600	2.0	0.04	1600

*Solid state TEA

burial and sediment mixing. In contrast to Scenario 1, however, physical mixing by macrofauna (bioturbation) is the dominant transport mechanism here, and a diffusion controlled exchange between the pore water and the biophase was not considered to be rate limiting. In addition, the formation of a biofilm or biophase was ignored in our simulations, and the microorganisms were assumed to have a direct access to both dissolved and solid chemical species.

The growth of each microbial group is described by Eqn. 1, with c_{DOC} as the concentration of the intermediate DOC pool. As in Scenario 1, oxygen was considered to be an inhibitor of anaerobic metabolic pathways. Again, the consumption of DOC, electron acceptors and the release of reaction products were related to microbial growth via the cell yield and the stoichiometry of the reactions. Bacterial decay was simulated using first order decay kinetics, the dead biomass being recycled to the organic carbon pool.

Values used for the parameters describing microbial growth and activity are listed in Table 3. Since most of these parameters could not be constrained from field data or experiments carried out on the site, the values used in Scenario 1 were adopted here with only slight modifications. In particular, we took into account that in Scenario 1, the simulated biomass build-up was probably too small (see Section 5.1). The maximum yield factors were therefore increased accordingly, while keeping the idea that they should decrease from the most favorable metabolic pathway (aerobic degradation) to the least favorable one (sulfate reduction). It was hypothesized that maximum growth rates are smaller in marine sediments than in the laboratory column experiments of Scenario 1, which was using lactate as highly labile carbon source. The latter were adjusted in such a way that the maximum substrate uptake rate (per unit biomass) of each process, given by $\frac{\mu_i}{Y_i}$, remained constant (Schäfer et al., 1998b). This scaling avoided the unrealistic situation where microorganisms with small yields consume the organic substrate faster than those having a higher yield. The decay rate of each organism was set to 1% of the fastest occurring maximum growth rate.

Values for the half saturation and inhibition constants were determined in an iterative manner to optimize the fitting of the measured concentration profiles and to avoid any significant accumulation of the intermediate DOC pool. Values of the "growth limiting concentrations" used by Wang and Van Cappellen (1996) were used here as initial guesses for the optimization process.

Due to fairly large uncertainties, the sensitivity of the model results to changes in microbial parameters was demonstrated here using two sets of values for both maximum growth and decay rates. A "reference case" was first simulated (Table 3), followed by a run where maximum growth and decay rates were increased by a factor of 10. The latter is further referred to as the "high activity case" and should be considered as an upper bound for the possible range of parameter values, since the kinetic constants for microbial growth and decay are of the same order of magnitude than those used for Scenario 1 (e.g., highest maximum growth rate of 365 y^{-1} in Scenario 1 and 100 y^{-1} in the high activity case of Scenario 3).

4. RESULTS

4.1. Scenario 1

A comparison of measured concentration profiles of dissolved chemical species after 48 days of column operation with the results of our simulations is shown in Figure 2. The target time of 48 days was chosen because the dataset is most complete for this sampling event. This was also the target time chosen in the modeling study of Schäfer et al. (1998b). Simulation results for solid chemical species correspond to the end of the experiment (110 days), when concentrations in the matrix were measured.

Results show that the model reproduces correctly the consumption of lactate, the production/consumption of propionate, as well as the production of acetate (Fig. 2). It captures also fairly well the instantaneous consumption of oxygen at the column inlet (results not shown) as well as the rapid consumption of nitrate. The measured concentration profiles show that sulfate was initially present in the entire column, with the zone of sulfate reduction slowly moving towards the column inlet during the course of the experiment. The model successfully reproduces this transient behavior (results not shown) with a sulfate reduction front positioned at ~5–10 cm from the column inlet after 48 days of operation (Fig. 2). The modeled increase in Mn(II) concentration over the entire column, the production and consumption of Fe(II) and of total sulfides, which are influenced by the combined effect of Fe(III) and

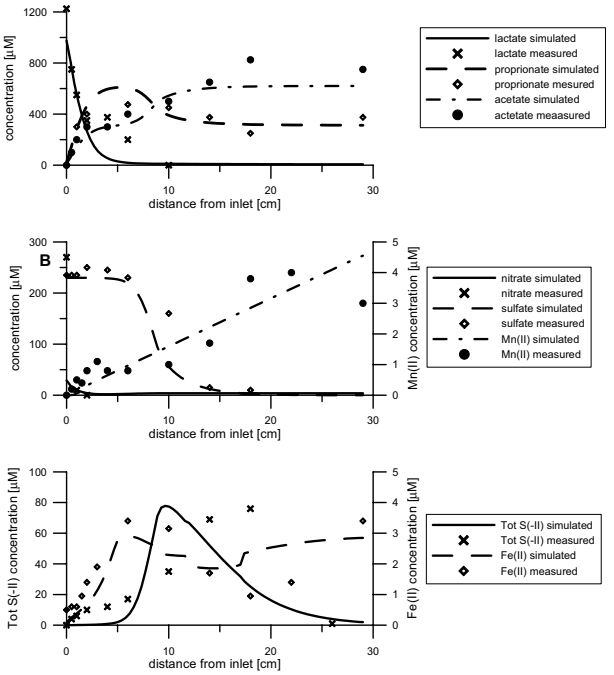

Fig. 2. Scenario 1: Comparison between simulated concentration profiles of dissolved chemical species after 48 days of column operation and measured data from von Gunten and Zobrist (1993) (as presented in Schäfer et al., 1998b). Tot S(-II) is the sum of dissolved sulfide species.

sulfate reduction and by the formation of Fe(II) minerals, are in overall agreement with the measured data, despite slight discrepancies in the 5–10 cm zone.

Measured concentration profiles for solid state Fe(II) and Fe(III) at the end of the experiment after 110 days of operation (Fig. 3) show a production of Fe(II) combined with a slight consumption of Fe(III) along the column, with the total concentration of solid Fe remaining nearly constant. These observations are nicely captured by the model, despite a slight overestimation of the rate of Fe(III) transformation into Fe(II) at around 10 cm from the column inlet.

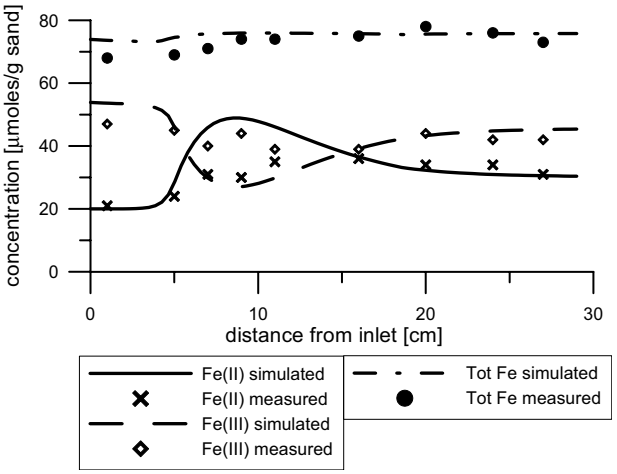

Fig. 3. Scenario 1: Comparison between simulated concentration profiles of solid chemical species after 110 days of column operation and measured data from von Gunten and Zobrist (1993) (as presented in Schäfer et al., 1998b). Tot Fe is the sum of solid state Fe(II) and Fe(III) species.

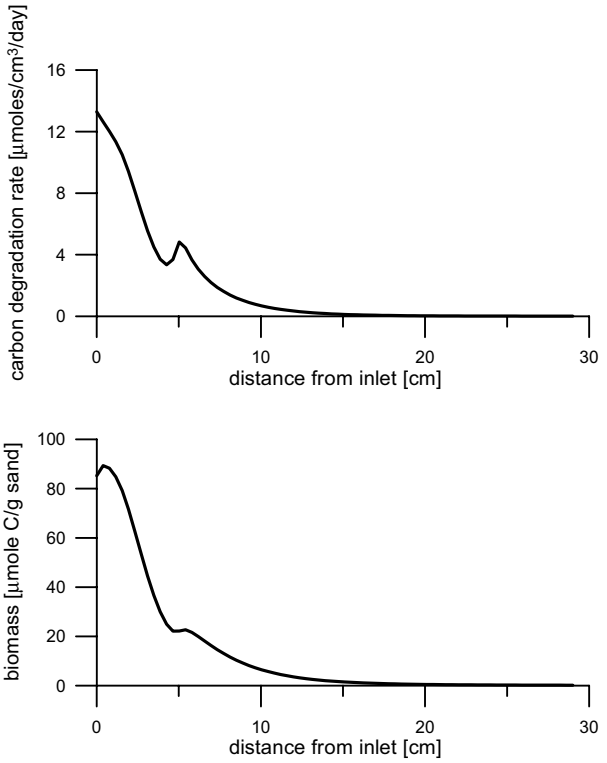

Fig. 4. Scenario 1: Simulated total carbon degradation rate and total biomass concentration profiles after 110 days of column operation.

The total carbon degradation rate profile simulated at the end of the experiment (day 110) show highest values at the column inlet followed by a sharp decrease within the first 10 cm (Fig. 4). Thereafter, the profile exhibits a small secondary peak, followed by a slower, smoother decrease with concentration reaching near-zero values at the column outlet. The total biomass concentration profile follows the same pattern, although the secondary peak observed in the rate profile is much smaller, here. The total amount of biomass integrated over the entire column at the end of the experiment is ~8 mmol C.

The simulated carbon oxidation rates follow a pattern of overlapping redox zones. A very similar spatial pattern is observed for the simulated longitudinal biomass distributions of the different bacterial groups (Fig. 5). Plotting redox reaction rates against the corresponding biomass concentrations shows that, for all microbial groups, high biomass concentrations correspond to high reaction rates. This relation is slightly less pronounced for the iron reducers, and for the sulfate reducers a hysteresis like pattern, that is, a non unique biomass—reaction rate relationship can be observed (Fig. 6; see Section 5.3).

4.2. Scenario 2

Measured and simulated steady state concentration profiles for Scenario 2 are shown in Figures 7 (dissolved chemical species) and 8 (solid chemical species). Model results match the observed consumption of oxygen within the top cm of the

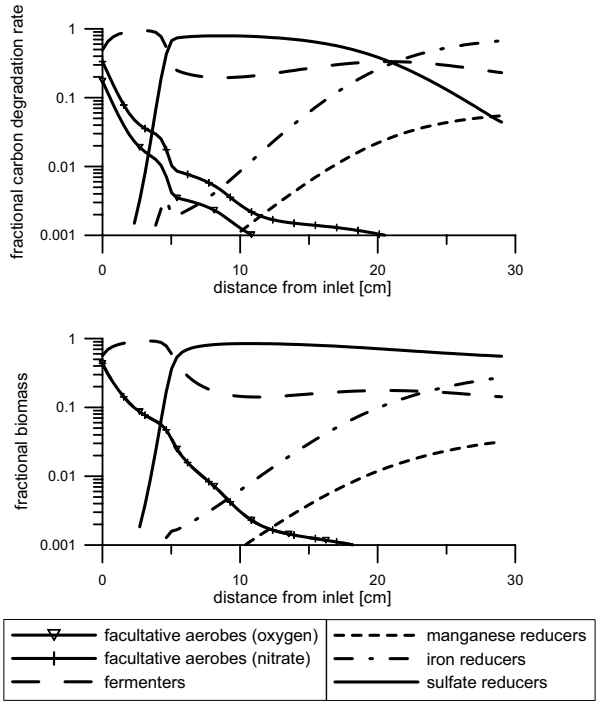

Fig. 5. Scenario 1: Simulated profiles of carbon degradation rates (as fraction of total rate) and concentration profiles of the associated microbial groups (as fraction of total biomass) after 110 days of column operation. Note that the facultative aerobes are one group of organisms controlling two different carbon degradation rates.

sediment, as well as the increase of Mn(II) and Fe(II) close to the sediment water interface followed by their subsequent decrease at greater depths. The simulations correctly reproduce the shallower increase in pore water Mn(II) compared to Fe(II).

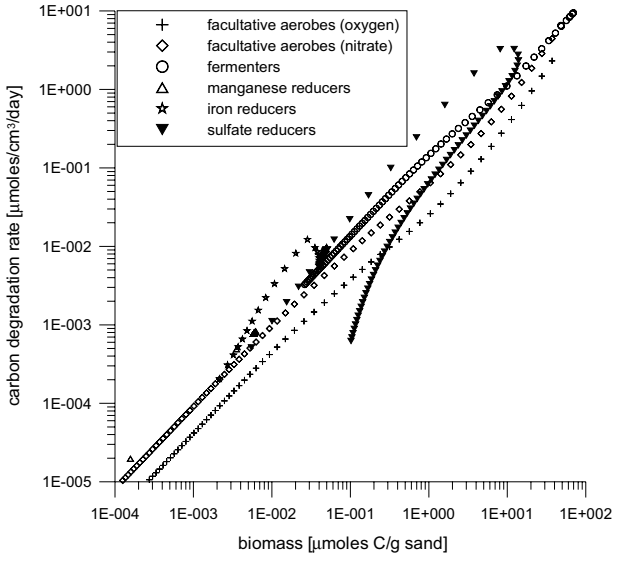

Fig. 6. Scenario 1: Simulated carbon degradation rates against the biomass concentration of the associated microbial groups after 110 days of column operation. Each symbol corresponds to a specific value of a specific grid cell.

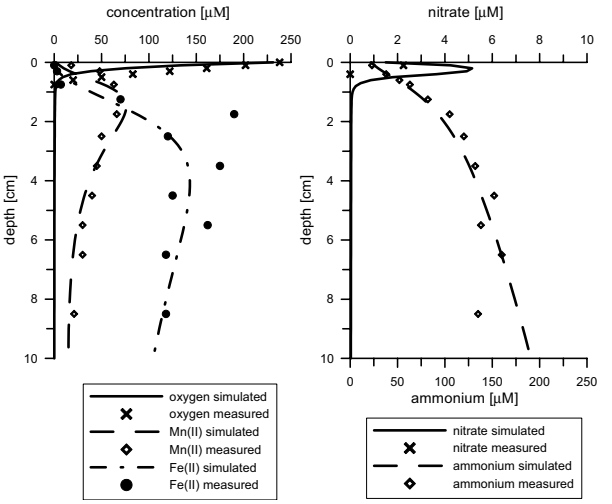

Fig. 7. Scenario 2: Comparison between simulated concentration profiles of dissolved chemical species and measured data from Canfield et al. (1993) (as presented in Wang and Van Cappellen, 1996).

The model predicts also a subsurface nitrate maximum, although the measured data points are too few to verify the presence of this feature. The profile of ammonium (released during the degradation of OM) is in good agreement with the data, showing a steady concentration increase with depth.

Concentration profiles of the measured solid chemical species are reproduced correctly by the model (Fig. 8). They indicate a consumption of MnO_2 and $Fe(OH)_3$ near the sediment-water interface followed by the formation of FeS and solid Fe(II) species ($FeCO_3$ and adsorbed Fe(II)) at greater depths. Finally, the total carbon oxidation rate simulated using the 1G-approach is nearly identical to the forcing function used by Wang and Van Cappellen (1996), which was fitted to carbon oxidation rates measured in short term sediment incubations (data not shown).

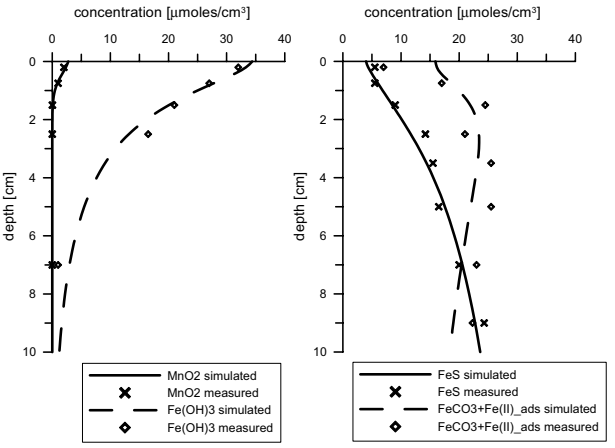

Fig. 8. Scenario 2: Comparison between simulated concentration profiles of solid chemical species and measured data from Canfield et al. (1993) (as presented in Wang and Van Cappellen, 1996).

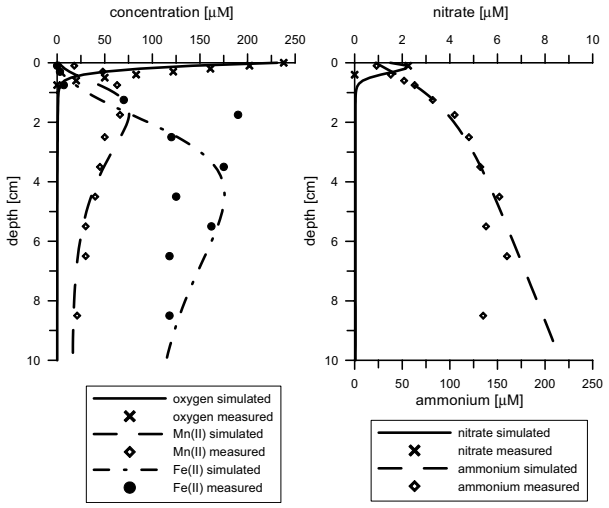

Fig. 9. Scenario 3: Comparison between simulated concentration profiles of dissolved chemical species and measured data from Canfield et al. (1993) (as presented in Wang and Van Cappellen, 1996).

4.3. Scenario 3

Results for the reference case of Scenario 3 show only minor differences with those of Scenario 2, which did not include microbial dynamics (Figs. 9 and 10). Differences can be observed for dissolved Fe(II) concentrations, which exhibit a larger increase in Scenario 3, and for nitrate concentrations, which are somewhat smaller. Results obtained for the high activity case demonstrate that when maximum growth and decay parameters are increased by a factor of 10, the predicted concentration profiles do not fundamentally change and measured concentration profiles are equally well reproduced (results not shown).

Simulated total carbon degradation rates are basically identical for the reference case and the high activity case and do not differ from the total rate simulated for Scenario 2 (Fig. 11). In the reference case, the simulated carbon oxidation rates exhibit steep gradients with depth (Fig. 12). In

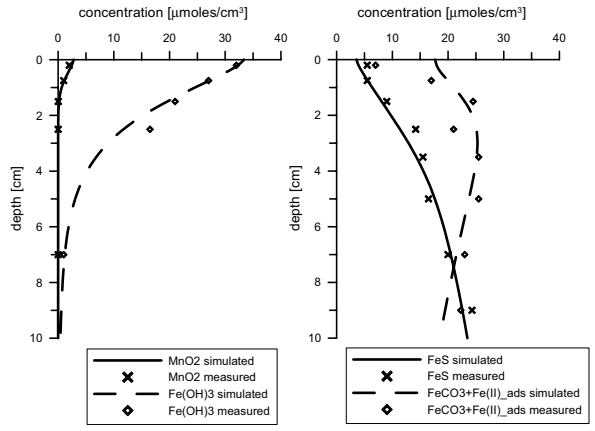

Fig. 10. Scenario 3: Comparison between simulated concentration profiles of solid chemical species and measured data from Canfield et al. (1993) (as presented in Wang and Van Cappellen, 1996).

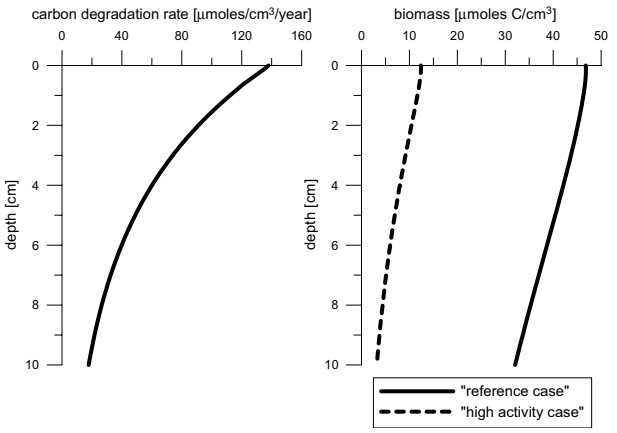

Fig. 11. Simulated total carbon degradation rate for Scenarios 2 and 3 and simulated total biomass concentration profile for Scenario 3. The carbon oxidation rates for the two scenarios are graphically indistinguishable.

contrast, very small spatial gradients can be observed for the biomass concentrations of the different microbial groups. As a result, for all microbial groups, high biomass concentrations are associated with a large range of the corresponding reaction rates (Fig. 13). In the high activity case, the spatial gradients of the biomass concentration profiles of the different microbial groups are slightly larger than those observed for the reference case (results not shown), yet high biomass concentrations still correspond to highly variable associated redox reaction rates (Fig. 14).

5. DISCUSSION

5.1. Performance of the BRNS

Our simulation results for Scenario 1 are nearly identical to those of Schäfer et al. (1998b), and indicate that the discrepancies between measured and simulated concentrations in the

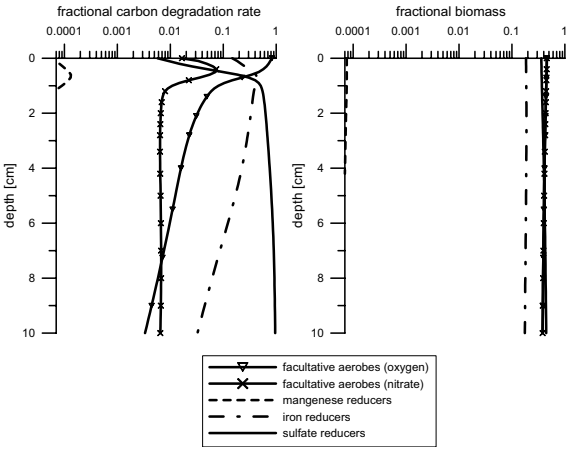

Fig. 12. Scenario 3: Simulated profiles of carbon degradation rates (as fraction of total rate) and concentration profiles of the associated microbial groups (as fraction of total biomass) obtained for the reference case. Note that the facultative aerobes are one group of organisms controlling two different carbon degradation rates.

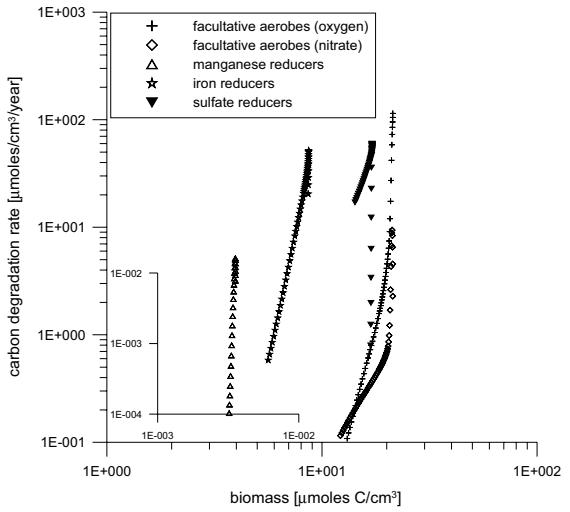

Fig. 13. Scenario 3: Simulated carbon degradation rates against the biomass concentration of the associated microbial groups obtained for the reference case. Each symbol corresponds to a specific value of a specific grid cell in the upper 10 cm of the sediment. Values for the manganese reducers refer to the inserted axes.

zone between 5 and 10 cm from the column inlet are likely due to processes not included or not adequately represented in the reaction network. The BRNS performs therefore equally well as the 'TBC' model of Schäfer et al. (1998a), a widely recognized reactive transport model in the area of contaminant hydrology (Thullner and Schäfer, 1999; Schäfer, 2001; Schäfer et al., 2003).

In the modeling study of Schäfer et al. (1998b), the predicted biomass growth in the column was not reported. However, von Gunten and Zobrist (1993) measured the protein concentration profile at the end of their experiment. Results showed highest concentration at the column inlet (~300 μg protein/g sand (wet)) followed by a decrease in the upper part of the column to values of ~ 100 μg protein/g sand (wet) at the outlet. These results cannot directly be compared with our modeled biomass concentration, given in μmol biomass C/g sand (dry), as the simulations only take into account the microbial strains associated with the primary redox reactions. Yet, von Gunten and Zobrist (1993) estimated the total amount of biomass in the column to be 25 mmol carbon, which is approximately three times higher than our model predictions. Possible reasons for this discrepancy are the presence of microorganisms not involved in the degradation of the injected carbon substrate and, hence, not included in our simulations, or the build-up of dead biomass in the column, while the model-based biomass only considers live cells. Alternatively, the assigned yield factors could have been too small. Nevertheless, the simulated biomass concentrations fall within a realistic range, and the overall pattern in biomass distribution is correctly reproduced by the BRNS.

A comparison between measured and simulated concentration profiles for Scenario 2 demonstrates that our model adequately reproduces the dataset of Canfield et al. (1993). Our reaction network is nearly identical to the one implemented in the RTM 'STEADYSED' (Van Cappellen and Wang, 1996), except for four parameter values that were adjusted to improve the fit to the measured data (see Table 2). The deviations between the output of the two models are nevertheless minor and, overall, the results obtained in this study are in very good agreement with those obtained with STEADYSED, a well established model for the simulation of early diagenetic processes in sediments (Wang and Van Cappellen, 1996; Furukawa et al., 2000; van den Berg et al., 2000).

The advantage of the BRNS approach is that it allows simulating these two reactive transport problems (representing contaminant hydrology and early diagenesis) within the same simulation environment. Furthermore, it should be noted that the flexibility of the BRNS is not limited to reaction networks presented in this study, but it allows, in fact, simulating an arbitrary set of mixed kinetic/equilibrium reactions.

5.2. Implementation of Biomass Growth into Early Diagenetic Models

Scenario 3 shows that the fit to the measured data remains essentially the same when the description of microbial growth used to simulate the column experiment is transferred to the early diagenetic application. The implementation of the coupling between organic matter degradation kinetics and microbial processes requires specification of yield factors and rate constants for microbial growth and decay, the values of which are poorly constrained by field or laboratory studies (Gasol and Duarte, 2000). In the high activity case, the simulated biomass concentrations are lower than in the reference case (Fig. 11). Nonetheless, both sets of parameters lead to comparably good fits of the measured inorganic concentration profiles. Largest differences between both model runs are observed for the simulated biomass concentration of manganese reducers and the associated carbon oxidation rate. However, measured concentration profiles for pore water and solid-phase manganese species are only slightly influenced by these differences, as manganese reduction contributes only little to total organic

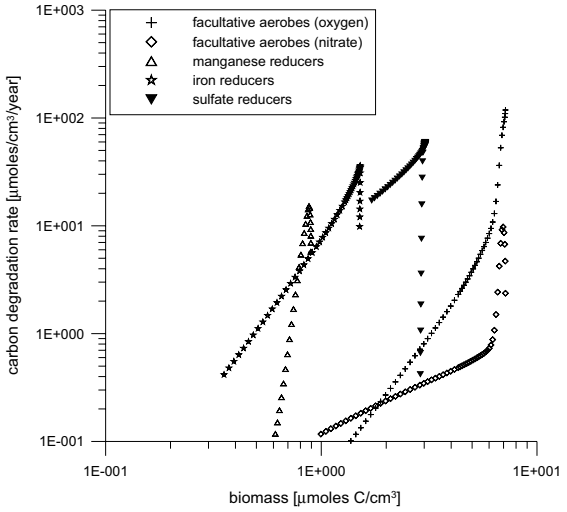

Fig. 14. Scenario 3: Simulated carbon degradation rates against the biomass concentration of the associated microbial groups obtained for the high activity case. Each symbol corresponds to a specific value of a specific grid cell in the upper 10 cm of the sediment.

carbon oxidation and the total manganese reduction is mainly driven by secondary reduction reactions.

The concentration profiles simulated with (Scenario 3) and without (Scenario 2) explicit incorporation of microbial growth show only minor differences. One possible reason for these similarities can be found in the 1G model approach, which leads to almost no feedback between the hydrolysis rate, microbial activity and redox reaction rates. This is in agreement with findings of previous studies (e.g., Westrich and Berner, 1984), which observed a dependency of the organic matter decomposition rate to added organic matter only. As a result of the 1G model, the bioavailable DOC and the sum of the primary redox reaction rates at any given depth do not differ between simulations. In Scenario 3, the recycling of dead bacterial biomass into degradable organic matter contributes to the carbon oxidation rates in the system. Yet, this contribution never exceeds 5% of the total carbon flux into the sediment, and is thus negligible. These conclusions are based on steady state simulations only, that is, they do no provide any information on how such steady states are reached. The investigation of the transient behavior and its sensitivity to the expressions and parameters used for describing redox reaction rates (e.g., Wirtz, 2003) should be addressed in future research. One can indeed assume that model predictions for the transient behavior of an early diagenetic system might significantly depend on whether the used reaction network considers an explicit link between microbial growth and redox reaction rates. For the column experiment, the simulation of the movement of reaction fronts would not be possible without including the impact of microbial growth. Extrapolating these findings to redox stratified environments would suggest that for the simulation of steady state or quasi-steady state systems a reaction network neglecting microbial growth might lead to acceptable simulation results, as shown in previous studies, whereas for a detailed understanding of processes controlling different degradation pathways as well as for simulating transient species distribution, a reaction network including microbial growth will be more appropriate than a reaction network without this feature.

All simulations yield vertical overlap of redox zones. In Scenario 2, the redox zonation and the extent of the overlap between degradation pathways of organic carbon utilizing different TEAs are entirely controlled by the inhibitory effect that each TEA exerts on the less favorable metabolic pathways (Eqn. 2). In Scenario 3, the competition of the microorganisms for the organic carbon substrates is the primary driving force for the redox stratification shown in Figure 12, oxygen being the only inhibitor in this simulation. This competition is mainly controlled by the relative concentrations of DOC and electron acceptors available at a given depth in the sediment, and the affinities of the microorganisms towards their growth limiting substrates (K_{TEA}, K_{DOC}), plus the group-specific growth rates (μ) and growth yields (Y). In addition, the different tolerance levels towards oxygen are influencing the competition among the bacterial groups.

In Scenario 1, different organic carbon species (lactate and propionate) are consumed by distinct bacterial groups (Table 1). This is an additional cause for the predicted redox zonation in the column experiment. In general, however, our results suggest that it is not necessary to impose ad hoc inhibition terms to generate a redox stratification; the competition for electron donors between different microbial groups offers an alternative, and more realistic, mechanism to explain the sequential utilization of TEAs. This demonstrates that including microbial activity in RTMs allows a more process oriented description of redox stratified aquatic sediments. Future research should now address whether expressions other than those of the Monod model proposed here could be used to explain microbially mediated redox reactions in sediments. For instance, in the field of contaminant hydrology, several kinetic approaches have been discussed recently as alternatives to the Monod model (e.g., Curtis, 2003; Watson et al., 2003), including e.g., a partial equilibrium approach (Jacobsen and Postma, 1999). Our results indicate that the outcome of these studies might be extrapolated to the field of early diagenesis.

5.3. Influence of Transport Regime on Redox Zonation and Microbial Community Structure

The spatial distribution of redox reaction rates for the three scenarios demonstrates that redox zonation arises regardless of the transport regime. This zonation is characterized by steep spatial gradients in the profiles of both rates and TEA concentrations. In contrast, concentration profiles of bacterial biomass show a strong dependency on the transport regime. In Scenario 1, transport of solutes is dominated by advection, while the biomass is attached on the immobile solid matrix. As a result, the biomass concentration of any given bacterial group at any given point along the flow path reflects the local reaction rate of the redox process(es) associated with this group. Such dynamics leads to a high spatial correlation between the distribution of the primary redox reaction rates and the concentration of the corresponding bacterial groups. As a result, a quantification of the biomass of different functional groups in such a system would allow the identification of the redox stratification in the system. It should be noted that if detachment and subsequent reattachment of the biomass in the column had been included in the model description, smoother biomass concentration gradients on the downstream side of the concentration peak would have been obtained. However, these processes are unlikely as the simulated total biomass concentration gradients show a similar pattern to those observed experimentally. Furthermore, von Gunten and Zobrist (1993) did not find any evidence that biomass was flushed out of the column during their experiment. Aside from bacterial detachment/attachment, the only other effect capable of weakening the predicted relationship between biomass concentrations and redox reaction rates is the transient movement of reaction fronts in the system. In case of sulfate, reduction the latter leads to a decaying yet viable bacterial population after the retreat of the reduction front. This explains the hysteresis like pattern found for the sulfate reducers. However, it should be noted that extrapolating the findings on the correlation between redox rates and biomass abundance to natural systems, such as an aquifer, might be challenged by the heterogeneity of the matrix material and the flow field (Nielsen et al., 1995a; Nielsen et al., 1995b).

In Scenario 3, transport of solutes is dominated by mixing processes (diffusion, bioturbation), while solids are transported mainly by bioturbation and to much less extent, by advection. Since it is hypothesized that microorganisms are associated with solids, transport also affects the microorganisms in this

scenario, a condition which results in a smooth distribution of the biomasses with depth. These homogeneous biomass concentration profiles are not correlated with the steep gradients observed for the redox reaction rates, and high biomass concentrations of a bacterial group do not indicate high rates of the associated reaction. Even in cases where biomass concentration and reaction rate exhibit a unique and monotonous relation, the accuracy of quantifying biomasses might be too small to allow the prediction of redox reaction rates from the biomass data. For instance, in the case of the facultative aerobes using oxygen as TEA, the marginal increase in biomass concentration from ~17 to 21 μmoles C/cm^3 corresponds to a change of the reaction rate by two orders of magnitude (Fig. 13). As a result, monitoring the biomass distribution of specific bacterial groups in surface sediments within the bioturbated zone may not provide useful information on the redox zonation of the system, despite the fact that the redox reactions depend on the abundance of the microorganisms. Besides transient effects, such as moving reaction fronts or changing boundary conditions, the relationship between biomass concentrations and associated reaction rates ultimately depends on the relative magnitude of the time scale for microbial growth and decay compared to the time scale for bioturbation. A small time scale for bioturbation combined with a large time scale for microbial decay lead to the observed homogeneous biomass distribution. In turn, sediments with large bioturbation time scales combined with small times scales for the decay of microorganisms might show a higher spatial correlation between redox rates and biomass abundance. In our case, the bioturbation coefficient of 20 cm^2 y^{-1} is within the typical range for such sites (Van Cappellen and Gaillard, 1996; Middelburg et al., 1997). Furthermore, increasing both the rates for microbial growth and decay does not lead to significantly different observations. These higher rates are only slightly smaller than the rates proposed for Scenario 1, which definitely constitutes an upper bound since it is not reasonable to assume that growth rates in marine sediments could exceed those observed in a column experiment characterized by a very high carbon load. Therefore, it can be concluded that the weak relationship between biomass distribution and redox reaction rates is likely to occur in many bioturbated systems. Measured data from marine and estuarine sediments are consistent with our simulations, with observations showing homogeneous biomass distributions in the presence of steep gradients in redox reaction rates (e.g., Oremland et al., 1984; Pallud and Van Cappellen, 2003; Koretsky et al., 2005). The finding of homogeneous biomass distributions in redox stratified systems provide a further explanation why early diagenetic models without explicit representation of microbial growth perform well in the reproduction of measured steady state concentration profiles of reactive chemical species.

The limitation of biomass activity due to restricted bioavailability of chemical species is another important control of the transport regime on the growth of bacterial biomass in porous media. For instance, the relatively high advection velocities in Scenario 1 limit the availability of reactants as well as the exchange rates between biophase and pore water, or biophase and solid matrix (see Schäfer et al. (1998b) for a detailed discussion). In turn, this limits the total activity of the microorganisms. In Scenario 3, a kinetically limited bioavailability was not considered since flow rates are small and mixing processes at the pore scale are sufficiently efficient to allow a direct, complete access of chemical species for the microorganisms. In this case, the total activity of the microorganisms is only limited by the bulk hydrolysis rate of organic matter.

6. SUMMARY AND CONCLUSIONS

A new and flexible simulation environment, the Biogeochemical Reaction Network Simulator (BRNS) has been applied to the simulation of reactive transport problems in groundwater environments and aquatic sediments. The BRNS performs equally well as previously established reactive-transport models (TBC and STEADYSED) dedicated to specific applications or specific porous environments described by different transport regimes and spatio-temporal scales. In contrast to TBC and STEADYSED, our approach addresses both problems within a single simulation environment.

Expressions for microbial growth and the explicit representation of the dependency of primary redox reaction rates on microbial activity were incorporated in a comprehensive biogeochemical reaction network for subsurface environments. The resulting geomicrobiological model captures the essential chemical dynamics and microbial colonization pattern observed in a sand column experiment, designed to investigate organic carbon degradation in an advective flow-dominated porous medium. The same modeling approach was then successfully transferred to the field of early diagenesis.

Our simulations predict a significant spatial correlation between microbial biomasses and redox reaction rates in the column experiment. This is a consequence of the advection-dominated solute-transport and the preferred attachment of the microorganisms to the immobile solid matrix. In surface sediments, mixing is the dominant transport mechanism acting on both solutes and solids. Such a transport regime homogenizes biomasses, which are no longer related to the steep spatial gradients in organic carbon oxidation rates, despite the fact that these rates are controlled by the microorganisms. The results demonstrate, therefore, that the relationship between microbial ecological structure of subsurface environments and the geochemical dynamics can only be fully understood in the framework of a reactive transport approach.

In important outcome of our study is to show that experimental data on the transient behavior of a biogeochemical system are most appropriate for deriving and testing mathematical formulations of microbially controlled reaction kinetics. In addition, the results emphasize that a quantitative description of the transport regime is necessary to decide whether measured microbial biomass distributions can be used as an indicator for the location of reaction zones in environmental systems.

Acknowledgments—Dirk Schäfer, University Kiel, Germany, is acknowledged for providing further information on the modeling study presented in Schäfer et al., 1998b. This study was funded by the Netherlands Organisation for Scientific Research (NWO) grant 813.02.008. An online IT-based version of the BRNS can be accessed via http://www.geo.uu.nl/~rtm/.

Associate editor: M. L. Machesky

REFERENCES

Aguilera D. R., Jourabchi P., Spiteri C., and Regnier P. (2005) A knowledge-based reactive transport approach for the simulation of

biogeochemical dynamics in earth systems. *Geochem. Geophys. Geosyst. (G^3)* **6,** Q07012.

Appelo C. A. J. and Postma D. (1993) Geochemistry, Groundwater and Pollution. A.A. Balkema, Rotterdam, The Netherlands.

Barry D. A., Prommer H., Miller C. T., Engesgaard P., Brun A., and Zheng C. (2002) Modelling the fate of oxidisable organic contaminants in groundwater. *Adv. Water Res.* **25,** 945–983.

Baurmann M., Ebenhöh W., and Feudel U. (2004) Turing instabilities and pattern formation in a benthic nutrient-microorganism system. *Math. Biosci. Eng.* **1,** 111–130.

Berg P., Rysgaard S., and Thamdrup B. (2003) Dynamic modeling of early diagenesis and nutrient cycling. A case study in an arctic marine sediment *Am. J. Sci.* **303,** 905–955.

Berner R. A. (1980) Early diagenesis: A theoretical approach. Princeton University Press, Princeton, NJ, USA.

Boudreau B. P. (1996) A method-of-lines code for carbon and nutrient diagenesis in aquatic sediments. *Comp. Geosci.* **22,** 479–496.

Brenan K. E., Campbell S. L., and Petzold L. R. (1989) Numerical Solution of Initial-Value Problems in Differential-Algebraic Systems. North Holland, Amsterdam, The Netherlands.

Brun A. and Engesgaard P. (2002) Modelling of transport and biogeochemical processes in pollution plumes: literature review and model development. *J. Hydrol.* **256,** 211–227.

Canfield D. E., Thamdrup B., and Hansen J. W. (1993) The anaerobic degradation of organic matter in Danish coastal sediments: iron reduction, manganese reduction and sulfate reduction. *Geochim. Cosmochim. Acta* **57,** 3867–3883.

Chapelle F. H (1992) *Ground-Water Microbiol. Geochem.* John Wiley & Sons, New York, NY, USA.

Chilakapati A. (1995) RAFT: A Simulator for Reactive Flow and Transport of Groundwater Contaminants. Pacific Northwest Laboratory, Internal Report 10636.

Curtis G. P. (2003) Comparison of approaches for simulating reactive solute transport involving organic degradation reactions by multiple electron acceptors. *Comp. Geosci.* **29,** 319–329.

Furukawa Y., Bentley S. J., Shiller A. M., Lavoie D. L., and Van Cappellen P. (2000) The role of biologically-enhanced pore water transport in early diagenesis: An example from carbonate sediments in the vicinity of North Key Harbor, Dry Tortugas National Park, Florida. *J. Mar. Res.* **58,** 493–522.

Gasol J. M. and Duarte C. M. (2000) Comparative analyses in aquatic microbial ecology: how far do they go? *FEMS Microb. Ecol.* **31,** 99–106.

Gomez C. (1990) MACROFORT: a FORTRAN code generator in MAPLE. Rapport Technique 119, INRIA.

Harter T. (2003) Basic Concepts of Groundwater Hydrology. University of California, Agriculture & Natural Resources, Publication No. 8083.

Hess A., Höhener P., Hunkeler D., and Zeyer J. (1996) Bioremediation of a diesel fuel contaminated aquifer: simulation studies in laboratory aquifer columns. *J. Contam. Hydrol.* **23,** 329–345.

Hindmarsh A. C. and Petzold L. R. (1995a) Algorithms and software for ordinary differential equations and differential/algebraic equations, Part 1: Euler methods and error estimation. *Comp. Phys.* **9,** 34–41.

Hindmarsh A. C. and Petzold L. R. (1995b) Algorithms and software for ordinary differential equations and differential/algebraic equations, Part 2: Higher-order methods and software packages. *Comp. Phys.* **9,** 148–155.

Hunter K. S., Wang Y., and Van Cappellen P. (1998) Kinetic modeling of microbially-driven redox chemistry of subsurface environments: coupling transport, microbial metabolism and geochemistry. *J. Hydrol.* **209,** 53–80.

Jakobsen R. and Postma D. (1999) Redox zoning, rates of sulfate reduction and interactions with Fe-reduction and methanogenesis in a shallow sandy aquifer, Rømø, Denmark. *Geochim. Cosmochim. Acta* **63,** 137–151.

Koretsky C. M., Moore C. M., Lowe K. L., Meile C., DiChristina T. J., and Van Cappellen P. (2003) Seasonal oscillation of microbial iron and sulfate reduction in saltmarsh sediments (Sapelo Island, GA, USA). *Biogeochem.* **64,** 179–203.

Koretsky C. M., Van Cappellen P., DiChristina T. J., Kostka J. E., Lowe K. L., Moore C. M., Roychoudhury A. N., and Violier E. (2005) Salt marsh pore water geochemistry does not correlate with microbial community structure. *Estuar. Coast. Shelf Sci.* **62,** 233–251.

Mayer K. U., Frind E. O., and Blowes D. W. (2002) Multicomponent reactive transport modeling in variably saturated porous media using a generalized formulation for kinetically controlled reactions. *Water Res. Res.* **38,** 1174.

Middelburg J. J., Soetaert K., and Herman P. M. J. (1997) Empirical relationships for use in global diagenetic models. *Deep-Sea Res. I* **44,** 327–344.

Monod J. (1949) The Growth of Bacterial Cultures. *Ann. Rev. Microbiol.* **3,** 371–394.

Murphy E. M. and Ginn T. R. (2000) Modeling microbial processes in porous media. *Hydrogeol. J.* **8,** 142–158.

Nielsen P. H., Albrechtsen, H.-J., Heron G., and Christensen T. H. (1995a) In situ and laboratory studies on the fate of specific organic compounds in an anaerobic landfill leachate plume, 1. Experimental conditions and fate of phenolic compounds *J. Contam. Hydrol.* **20,** 27–50.

Nielsen P. H., Bjarnadottir H., Winter P. L., and Christensen T. H. (1995b) In situ and laboratory studies on the fate of specific organic compounds in an anaerobic landfill leachate plume, 2. Fate of aromatic and chlorinated aliphatic compounds *J. Contam. Hydrol.* **20,** 51–66.

Oremland R. S., Umberger C., Culbertsen C. W., and Smith R. L. (1984) Denitrification in San Francisco Bay intertidal sediments. *Appl. Env. Microbiol.* **47,** 1106–1112.

Pallud C. and Van Cappellen P. (2003) Kinetic study of sulfate reduction in estuarine sediments. *Geophys. Res. Abstr.* **5,** EGS-AGU-EUG Joint Assembly, Nice, France, April 6–11.

Press W., Flannery B., Teukolsky S., and Vetterling W (1992) Numerical Recipes in Fortran: the Art of Scientific Computing. Cambridge University Press, Cambridge, UK.

Prommer H., Barry D. A., and Zheng C. (2003) MODFLOW/MT3DMS-based reactive multicomponent transport modeling. *Ground Water* **41,** 247–257.

Ravenschlag K., Sahm K., Knoblauch C., Jorgensen B. B., and Amann R. (2000) Community structure, cellular rRNA content and activity of sulfate-reducting bacteria in marine arctic sediments. *Appl. Env. Microbio.* **66,** 3592–3602.

Regnier P., Wollast R., and Steefel C. I. (1997) Long-term fluxes of reactive species in macrotidal estuaries: estimates from a fully transient, multi-component reaction transport model. *Mar. Chem.* **58,** 127–145.

Regnier P., O'Kane J. P., Steefel C. I., and Vanderborght J. P. (2002) Modeling complex multi-component reactive transport systems: towards a simulation environment based on the concept of a Knowledge Base. *Appl. Math. Model.* **26,** 913–927.

Regnier P., Jourabchi P., and Slomp C. P. (2003) Reactive-transport modeling as a technique for understanding coupled biogeochemical processes in surface and subsurface environments. *Neth. J. Geosci.* **82,** 5–18.

Roose-Amsaleg C. L., Garnier-Sillam E., and Harry M. (2001) Extraction and purification of microbial DNA from soil and sediment samples. *Appl. Soil Ecol.* **18,** 47–60.

Sass H., Cypionka H., and Babanzien H.-D. (1997) Vertical distribution of sulfate reducing bacteria at the oxic anoxic interface in sediments of the oligotrophic Lake Stechlin. *FEMS Microbio. Eco.* **22,** 245–255.

Schäfer D., Schäfer W., and Kinzelbach W. (1998a) Simulation of reactive processes related to biodegradation in aquifers: 1. Structure of the three-dimensional reactive transport model *J. Contam. Hydrol.* **31,** 167–186.

Schäfer D., Schäfer W., and Kinzelbach W. (1998b) Simulation of reactive processes related to biodegradation in aquifers: 2. model application to a column study on organic carbon degradation *J. Contam. Hydrol.* **31,** 187–209.

Schäfer W. (2001) Predicting natural attenuation of xylene in groundwater using a numerical model. *J. Contam. Hydrol.* **52,** 57–83.

Schäfer D., Köber R., and Dahmke A. (2003) Competing TCE and cis-DCE degradation kinetics by zero-valent iron – experimental results and numerical simulation. *J. Contam. Hydrol.* **65,** 183–202.

Smets B. F. and Pritchard P. H. (2003) Elucidating the microbial component of natural attenuation. *Curr. Op. Biotech.* **14,** 283–288.

Soetaert K., Herman P. M. J., and Middelburg J. J. (1996) A model of early diagenetic processes from the shelf to abyssal depths. *Geochim. Cosmochim. Acta* **60,** 1019–1040.

Steefel C. I. and MacQuarrie K. T. B. (1996) Approaches to modeling of reactive-transport in porous media. In *Reactive Transport in Porous Media* (eds. P. C. Lichtner, C. I. Steefel and E. H. Oelkers) *Rev. Mineral.* **34**, 83–129.

Talin F., Tolla C., Rabouille C., and Poggiale J. C. (2003) Relations between bacterial biomass and carbon cycle in marine sediments: an early diagenetic model. *Acta Biotheoret.* **51,** 295–315.

Thullner M. and Schäfer W. (1999) Modeling of a field experiment on bioremediation of chlorobenzenes in groundwater. *Bioremed. J.* **3,** 247–267.

van Breukelen B. M., Griffioen J., Röling W. F. M., and van Versefeld H. W. (2004) Reactive transport modelling of biogeochemical processes and carbon isotope geochemistry inside a landfill leachate plume. *J. Contam. Hydrol.* **70,** 249–269.

Van Cappellen P. and Gaillard J.-F. (1996) Biogeochemical dynamics in aquatic sediments. In *Reactive Transport in Porous Media* (eds. P. C. Lichtner, C. I. Steefel and E. H. Oelkers) *Rev. Mineral.* **34**, 335–376.

Van Cappellen P. and Wang Y. (1996) Cycling of iron and manganese in surface sediments: a general theory for the coupled transport and reaction of carbon, oxygen, nitrogen, sulfur, iron and manganese. *Am. J. Sci.* **296,** 197–243.

van den Berg G. A., Loch J. P. G., van der Heijdt L. M., and Zwolsman J. J. G. (2000) Redox processes in recent sediments of the river Meuse, The Netherlands. *Biogeochem.* **48,** 217–235.

von Gunten U. and Zobrist J. (1993) Biogeochemical changes in groundwater-infiltrations systems: column studies. *Geochim. Cosmochim. Acta* **57,** 3895–3906.

Wang Y. and Van Cappellen P. (1996) A multicomponent reactive transport model of early diagenesis: application to redox cycling in coastal marine sediments. *Geochim. Cosmochim. Acta* **60,** 2993–3014.

Watson I. A., Oswald S. E., Mayer K. U., Wu X., and Banwart S. A. (2003) Modeling kinetic processes controlling hydrogen and acetate concentrations in an aquifer-derived microcosm. *Env. Sci. Technol.* **37,** 3910–3919.

Westrich J. T. and Berner R. A. (1984) The role of sedimentary organic matter in bacterial sulfate reduction: The G model tested. *Limnol. Oceanogr.* **29,** 236–249.

Wieringa E. B. A., Overmann J., and Cypionka H. (2000) Detection of abundant sulphate-reducing bacteria in marine oxic sediment layers by a combined cultivation and molecular approach. *Env. Microbiol.* **2,** 417–427.

Wirtz K. W. (2003) Control of biogeochemical cycling by mobility and metabolic strategies of microbes in the sediments: an integrated model study. *FEMS Microbiol. Ecol.* **46,** 295–306.

Zarda B., Mattison G., Hess A., Hahn D., Höhener P., and Zeyer J. (1998) Analysis of bacterial and protozoan communities in an aquifer contaminated with monoaromatic hydrocarbons. *FEMS Microbiol. Ecol.* **27,** 141–152.

APPENDIX 1.

Equations used for the simulation of the primary redox processes in the different scenarios. Rates and stoichiometries of all other reactions listed in Table 1 are described in Schäfer et al. (1998b) for Scenario 1 and Van Cappellen and Wang (1996) for Scenarios 2 and 3.

Scenario 1: Organic carbon degradation pathways and rates as given by Schäfer et al. (1998b):

Pathway	Stoichiometry	Degradation rate (per mol carbon)
Aerobic degradation	$C_3H_5O_3^-(lac) + 3O_2 \rightarrow 3HCO_3^- + 2H^+$	$r = \frac{\mu_{fac_{O2}}}{Y_{O2}} \cdot \frac{c_{lac}}{K_{bc}+c_{bc}} \cdot \frac{c_{O2}}{K_{O2}+c_{O2}} \cdot B_{fac}$
Denitrification	$5C_3H_5O_3^-(lac) + 12NO_3^- + 2H^+ \rightarrow 15HCO_3^- + 6N_2 + 6H_2O$	$r = \frac{\mu_{fac_{NO3}}}{Y_{NO3}} \cdot \frac{c_{lac}}{K_{loc}+c_{lac}} \cdot \frac{c_{NO3}}{K_{NO3}+c_{NO3}} \cdot \frac{K_{inh}}{K_{inh}+c_{O2}} \cdot B_{fac}$
Fermentation	$3C_3H_5O_3^-(lac) \rightarrow 2C_3H_5O_2^-(prop) + C_2H_3O_2^-(ac) + HCO_3^- + H^+$	$r = \frac{\mu_{ferm}}{Y_{ferm}} \cdot \frac{c_{lac}}{K_{lac}+c_{lac}} \cdot \frac{K_{inh}}{K_{inh}+c_{O2}} \cdot B_{ferm}$
Manganese reduction	$C_3H_5O_2^-(prop) + 7MnO_2 + 12H^+ \rightarrow 3HCO_3^- + 7Mn^{2+} + 7H_2O$	$r = \frac{\mu_{MnO2}}{Y_{MnO2}} \cdot \frac{c_{prop}}{K_{prop}+c_{prop}} \cdot \frac{c_{MnO2}}{K_{MnO2}+c_{MnO2}} \cdot \frac{K_{inh}}{K_{inh}+c_{O2}} \cdot B_{MnO2}$
Iron reduction	$C_3H_5O_2^-(prop) + 14FeOOH + 26H^+ \rightarrow 3HCO_3^- + 14Fe^{2+} + 21H_2O$	$r = \frac{\mu_{FeOOH}}{Y_{FeOOH}} \cdot \frac{c_{prop}}{K_{prop}+c_{prop}} \cdot \frac{c_{FeOOH}}{K_{FeOOH}+c_{FeOOH}} \cdot \frac{K_{inh}}{K_{inh}+c_{O2}} \cdot B_{FeOOH}$
Sulfate reduction	$4C_3H_5O_2^-(prop) + 3SO_4^{2-} \rightarrow 4HCO_3^- + 3HS^- + H^+ + 4C_2H_3O_2^-(ac)$	$r = \frac{\mu_{SO4}}{Y_{SO4}} \cdot \frac{c_{prop}}{K_{prop}+c_{prop}} \cdot \frac{c_{SO4}}{K_{SO4}+c_{SO4}} \cdot \frac{K_{inh}}{K_{inh}+c_{O2}} \cdot B_{SO4}$

Bacterial growth rates as given by Schäfer et al. (1998b):

Facultative aerobes:
$$\frac{\partial B_{fac}}{\partial t} = \left(\mu_{fac_{O2}} \frac{c_{lac}}{K_{lac}+c_{lac}} \cdot \frac{c_{O2}}{K_{O2}+c_{O2}} + \mu_{fac_{NO3}} \frac{c_{lac}}{K_{lac}+c_{lac}} \cdot \frac{c_{NO3}}{K_{NO3}+c_{NO3}} \cdot \frac{K_{inh}}{K_{inh}+c_{O2}} - \mu_{dec,fac} \right) \cdot B_{fac}$$

Fermentative bacteria:
$$\frac{\partial B_{ferm}}{\partial t} = \left(\mu_{ferm} \frac{c_{lac}}{K_{lac}+c_{lac}} \cdot \frac{K_{inh}}{K_{inh}+c_{O2}} - \mu_{dec,ferm} \right) \cdot B_{ferm}$$

Manganese reducers:
$$\frac{\partial B_{MnO2}}{\partial t} = \left(\mu_{MnO2} \frac{c_{prop}}{K_{prop}+c_{prop}} \cdot \frac{c_{MnO2}}{K_{MnO2}+c_{MnO2}} \cdot \frac{K_{inh}}{K_{inh}+c_{O2}} - \mu_{dec,MnO2} \right) \cdot B_{MnO2}$$

Iron reducers:
$$\frac{\partial B_{FeOOH}}{\partial t} = \left(\mu_{FeOOH} \frac{c_{prop}}{K_{prop}+c_{prop}} \cdot \frac{c_{FeOOH}}{K_{FeOOH}+c_{FeOOH}} \cdot \frac{K_{inh}}{K_{inh}+c_{O2}} - \mu_{dec,FeOOH} \right) \cdot B_{FeOOH}$$

Appendix 1. (Continued)

Sulfate reducers:

$$\frac{\partial B_{SO4}}{\partial t} = \left(\mu_{SO4}\frac{c_{prop}}{K_{prop}+c_{prop}}\cdot\frac{c_{SO4}}{K_{SO4}+c_{SO4}}\cdot\frac{K_{inh}}{K_{inh}+c_{O2}} - \mu_{dec,\,SO4}\right)\cdot B_{SO4}$$

Scenario 2: Organic carbon degradation pathways and rates as given by Van Cappellen and Wang (1996) (f_i as defined by Eqn. 2, CO_2 stands for dissolved CO_2; the Redfield ratio is x/y/z = 106/12/1):

Pathway	Stoichiometry	Degradation rate (per mol carbon)
Aerobic degradation	$(CH_2O)_x(NH_3)_y(H_3PO_4)_z + (x + 2y)O_2 + (y + 2z)HCO_3^- \rightarrow (x + y + 2z)CO_2 + yNO_3^- + zHPO_4^{2-} + (x + 2y + 2z)H_2O$	$r = k_C \cdot c_{CH2O} \cdot f_{O2}$
Denitrification	$5(CH_2O)_x(NH_3)_y(H_3PO_4)_z + (4x + 3y)NO_3^- \rightarrow (2x + 4y)N_2 + (x - 3y + 10z)CO_2 + (4x + 3y - 10z)HCO_3^- + 5zHPO_4^{2-} + (3x + 6y + 10z)H_2O$	$r = k_C \cdot c_{CH2O} \cdot f_{NO3}$
Manganese reduction	$(CH_2O)_x(NH_3)_y(H_3PO_4)_z + 2xMnO_2 + (3x + y - 2z)CO_2 + (x + y - 2z)H_2O \rightarrow 2xMn^{2+} + (4x + y - 2z)HCO_3^- + yNH_4^+ + zHPO_4^{2-}$	$r = k_C \cdot c_{CH2O} \cdot f_{MnO2}$
Iron reduction	$(CH_2O)_x(NH_3)_y(H_3PO_4)_z + 4xFe(OH)_3 + (7x + y - 2x)CO_2 \rightarrow 4xFe^{2+} + (8x + y - 2z)HCO_3^- + yNH_4^+ + zHPO_4^{2-} + (3x - y + 2z)H_2O$	$r = k_C \cdot c_{CH2O} \cdot f_{FeOH3}$
Sulfate reduction	$2(CH_2O)_x(NH_3)_y(H_3PO_4)_z + xSO_4^{2-} + 2(y - 2z)CO_2 + 2(y - 2z)H_2O \rightarrow xH_2S + 2(x + y - 2z)HCO_3^- + 2yNH_4^+ + 2zHPO_4^{2-}$	$r = k_C \cdot c_{CH2O} \cdot f_{SL04}$

Scenario 3: Organic carbon degradation pathways and rates (CO_2 stands for dissolved CO_2; the Redfield ratio is x/y/z = 106/12/1) Note that values for the inhibition constant for oxygen (K_{inh}) are pathway specific:

Pathway	Stoichiometry	Degradation rate (per mol carbon)
Hydrolysis	$(CH_2O)_x(NH_3)_y(H_3PO_4)_z(OM) + (y - 2z)H^+ \rightarrow xCH_2O(DOC) + yNH_4^+ + zHPO_4^{2-}$	$r = k_C \cdot c_{OM}$
Aerobic degradation	$CH_2O(DOC) + O_2 \rightarrow CO_2 + H_2O$	$r = \frac{\mu_{fac_{O2}}}{Y_{O2}}\cdot\frac{c_{DOC}}{K_{DOC}+c_{DOC}}\cdot\frac{c_{O2}}{K_{O2}+c_{O2}}\cdot B_{fac}$
Denitrification	$5CH_2O(DOC) + 4NO_3^- \rightarrow 2N_2 + CO_2 + 4HCO_3^- + 3H_2O$	$r = \frac{\mu_{facNO3}}{Y_{NO3}}\cdot\frac{c_{DOC}}{K_{DOC}+c_{DOC}}\cdot\frac{c_{NO3}}{K_{NO3}+c_{NO3}}\cdot\frac{K_{inh}}{K_{inh,\,NO}+c_{O2}}\cdot B_{fac}$
Manganese reduction	$CH_2O(DOC) + 2MnO_2 + 3CO_2 + H_2O \rightarrow 2Mn^{2+} + 4HCO_3^-$	$r = \frac{\mu_{MnO2}}{Y_{MnO2}}\cdot\frac{c_{DOC}}{K_{DOC}+c_{DOC}}\cdot\frac{c_{MnO2}}{K_{MnO2}+c_{MnO2}}\cdot\frac{K_{inh}}{K_{inh}+c_{O2}}\cdot B_{MnO2}$
Iron reduction	$CH_2O(DOC) + 4Fe(OH)_3 + 7CO_2 \rightarrow 4Fe^{2+} + 8HCO_3^- + 3H_2O$	$r = \frac{\mu_{FeOH3}}{Y_{FeOH3}}\cdot\frac{c_{DOC}}{K_{DOC}+c_{DOC}}\cdot\frac{c_{FeOH3}}{K_{FeOH3}+c_{FeOH3}}\cdot\frac{K_{inh}}{K_{inh}+c_{O2}}\cdot B_{FeOH3}$
Sulfate reduction	$2CH_2O(DOC) + SO_4^{2-} \rightarrow H_2S + 2HCO_3^-$	$r = \frac{\mu_{SO4}}{Y_{SO4}}\cdot\frac{c_{DOC}}{K_{DOC}+c_{DOC}}\cdot\frac{c_{SO4}}{K_{SO4}+c_{SO4}}\cdot\frac{K_{inh}}{K_{inh}+c_{O2}}\cdot B_{SO4}$

Bacterial growth rates:

Facultative aerobes:

$$\frac{\partial B_{\mathrm{fac}}}{\partial t} = \left(\mu_{fac_{O2}}\frac{c_{DOC}}{K_{DOC}+c_{DOC}}\cdot\frac{c_{O2}}{K_{O2}+c_{O2}} + \mu_{fac_{NO3}}\frac{c_{DOC}}{K_{DOC}+c_{DOC}}\cdot\frac{c_{NO3}}{K_{NO3}+c_{NO3}}\cdot\frac{K_{inh}}{K_{inh}+c_{O2}} - \mu_{dec}\right)\cdot B_{fac}$$

Manganese reducers:

$$\frac{\partial B_{MnO2}}{\partial t} = \left(\mu_{MnO2}\frac{c_{DOC}}{K_{DOC}+c_{DOC}}\cdot\frac{c_{MnO2}}{K_{MnO2}+c_{MnO2}}\cdot\frac{K_{inh}}{K_{inh}+c_{O2}} - \mu_{dec}\right)\cdot B_{MnO2}$$

Iron reducers:

$$\frac{\partial B_{FeOH3}}{\partial t} = \left(\mu_{FeOH3}\frac{c_{DOC}}{K_{DOC}+c_{DOC}}\cdot\frac{c_{FeOH3}}{K_{FeOH3}+c_{FeOH3}}\cdot\frac{K_{inh}}{K_{inh}+c_{O2}} - \mu_{dec}\right)\cdot B_{FeOH3}$$

Sulfate reducers:

$$\frac{\partial B_{SO4}}{\partial t} = \left(\mu_{SO4}\frac{c_{DOC}}{K_{DOC}+c_{DOC}}\cdot\frac{c_{SO4}}{K_{SO4}+c_{SO4}}\cdot\frac{K_{inh}}{K_{inh}+c_{O2}} - \mu_{dec}\right)\cdot B_{SO4}$$